Microscopic characterization of different shrinkage defects in ductile irons and their relation with composition and inoculation process

Anna Regordosa[1,2] and Núria Llorca-Isern[2]
1 Departament de Metal·lúrgia, Fundería Condals, S. A., E-08241 Manresa (Spain).
2 Departament de Ciència dels Materials I Enginyeria Metal·lúrgica, Universitat de Barcelona, E-08028 Barcelona (Spain).

ABSTRACT

Shrinkage becomes one of the most important defects that negatively affect the production of ductile cast iron parts. Regular inspections made on the affected parts show that different morphologies of shrinkage can be obtained according to the melt composition, to the layout and to a number of other processing variables that have been reported in the literature. However, minimization of these defects demands a more detailed understanding of their internal features and the relation with the most affecting processing variables. In the present study, carbon equivalent content, inoculation and thermal characterization of melts have been studied as variables for producing eight test parts which have been designed for promoting the formation of shrinkage. The different defects obtained in each case have been then analyzed by means of metallographic techniques and FE-SEM and their characteristics and size correlated to the selected variables. It has been found that carbon equivalent shows the strongest effect on shrinkage incidence. A discussion about the features found in the internal surfaces of the different closed defects is done and possible explanations for each case are also described.

Keywords: ductile cast iron, shrinkage, inoculation, carbon equivalent, solidification, scanning electron microscope, dendrites

INTRODUCTION

Shrinkage porosity becomes one of the most relevant defects commonly found in ductile cast iron parts. As production costs and other quality related problems increase due to shrinkage detection in castings, numerous efforts are usually made in foundries to avoid the appearance of such internal defects. However, complex design of parts and process instabilities usually makes such target difficult as contraction of solidifying alloys is known to depend on processing parameters and on chemical composition. Description of shrinkage occurrence in cast irons and of its characteristics becomes complex because they are the result of both graphite expansion and metallic contraction during the different steps of solidification[1].

Numerous works have been published about the formation mechanisms of shrinkage defects in spheroidal graphite cast irons and about its relation with some structural and chemical features. In this way, several studies have been focused on inoculation process[2-6] to minimize the risk of shrinkage formation in cast parts. Consequently, new inoculant compositions have been proposed for promoting graphite nucleation sites during the whole solidification range and for increasing graphite expansion.

Larrañaga et al.[3] experimentally studied how carbon and silicon contents are relevant variables for promoting graphite precipitation as these two elements showed an effect similar to the one expected from inoculants. They observed that hypereutectic compositions promote early graphite nucleation and growth which change the solidification sequence and a reduction of the risk of contraction defects formation is obtained.

Kanno et al.[7] analyzed the effect of a number of processing variables on shrinkage in order to minimize the formation of these defects in spheroidal graphite cast iron parts. They found a high risk of microshrinkage formation and growth when increasing the pouring temperature. In such work, it was also observed that the minimum shrinkage incidence occurred near the eutectic composition while dendritic and smooth porosities were respectively found for hypoeutectic and for hypereutectic compositions. The contraction defects obtained for hypereutectic compositions were related to an increase of primary graphite crystallization and thus to a decreased amount of graphite formed during the bulk eutectic solidification.

The effect of other processing variables like nodule count[8,9], feeder systems management[4], mold rigidity[5,10] and magnesium content[5] on shrinkage appearance has also been investigated. Some of these works additionally show relevant effects on this defect coming from other variables like carbon content[3].

Although shrinkage features have been the subject of many researchers, results are not similar in an important number of cases. An example of this controversy is the nodule count[11] for which both positive[6,8,9,12] and negative[5,13] effects on shrinkage avoidance have been reported. Also, prediction models have been developed as a result of some of these studies,[8,9,14-16] for evaluating the shrinkage tendency of produced castings.

The present work shows the results obtained from detailed characterizations made on shrinkage detected in test castings that were produced using different melt compositions, inoculant additions and pouring temperatures. This research has led to relating the different morphological features found in the contraction porosities to chemical composition and to inoculation condition. A comparative discussion concerning the defects characterization and their possible causes is also made in terms of solidification process.

EXPERIMENTAL WORK

Eight different ductile iron alloys were prepared to manufacture test parts which were designed in order to obtain contraction defects in the last solidifying areas (Fig. 1). The massive zone of the test part is connected to a feeder by means of a horizontal thin wall path. Thus, an effective feeding process is not expected for an important period of the solidification due to the thin section of this wall-shaped area. The highest risk of shrinkage appearance is thus expected to form in the last solidifying zone. The weight of each assembly composed by the test part and the riser is 4 kg.

Base melts were prepared in a 6 t capacity medium frequency induction furnace (250 Hz, 4250 kW). Metallic charges mainly composed by steel scrap and foundry returns were introduced in the furnace crucible when a remaining amount of melt (around 4000 kg) was already present in. After melting the chemical composition of the melt was adjusted by adding the needed amounts of

graphite and FeSi (75.2 wt. % Si, 0.7 wt. % Al and 0.3 wt. % Ca). Then temperature was increased up to 1500ºC and around 2000 kg of the base alloy were transferred to a ladle for treating it with a commercial FeSiMg alloy (45.4 wt.% Si, 3.0 wt.% Ca, 9.2 wt.% Mg, 2.9 wt.% rare earth) by means of the sandwich method using steel scrap as covering material.

Once the Mg-treatment was finished the batches were properly skimmed and then introduced into a pouring unit with pressurized nitrogen and with a heater system. Chemical composition of the different Mg-treated alloys was determined by analyzing melt samples that were picked up from the pouring basin during the production of the test parts. These analyses were performed using a combustion technique for carbon and sulfur contents and Spark Emission Spectroscopy for the rest of elements. Melt samples were also picked up in the pouring basin for filling two standard thermal analysis (TA) cups and for recording the corresponding cooling curves. One of the TA cups contained the same percentage as the sample of a commercial inoculant (grain size 0.2-0.7 mm, 70.5 wt. % Si, 3.7 wt. % Al, 1.03 wt. % Ca) before the addition of the liquid alloy while the other cup was a plain one.

Green sand molds were produced in a high pressure automatic vertical molding line. Inoculation of melts was made just before pouring the molds by adding different amounts of the commercial inoculant described above by means of a tube which was oriented to the melt stream when filling the molds. These additions were calculated as percentage of inoculant with respect to the total amount of melt poured in the mold (25 kg). The non inoculated test parts were produced avoiding any addition of inoculant to the pouring stream. After producing the test parts, they were cut in half to reveal the internal porosities formed after solidification. The area of all porosities present in the half test parts was measured using an image analysis software. A shrinkage area was finally obtained per test part.

Metallographic characterization was performed on 10×10 mm samples which were obtained from the central area of test parts, i.e. the expected last solidifying zone. Nodularity, nodule count and fraction of the different structural constituents present in the metallic matrix were determined on these samples. For this purpose, six different fields were inspected at 100x magnification per sample and average values in case of carbides fraction (f_c), ferrite fraction (f_α) and pearlite fraction (f_p) were determined after etching the samples with Nital 4% reagent. The maximum and the minimum values of nodule count have also been determined.

Internal morphologies of shrinkage defects were analyzed with a FESEM equipment with observation conditions of ΔV=20 kV, WD= 10 mm and intensity probe of 4.5 nA. Secondary electron mode (SE Image) and backscattered electron mode (BSE Image) techniques were used for characterizing the composition of these contraction defects.

Table 1 shows the results of the chemical composition analyses performed on the eight cast irons prepared in the present study. This table also includes the inoculant additions in each case and the pouring temperatures. Note that both hypoeutectic (HO) and hypereutectic (HR) compositions were used for producing the test parts with four inoculated alloys which have been marked as "-I" and with four non inoculated alloys denoted as "-NI". Last numbers in codes used in Table 1 refers to

the part number. Although the same inoculant addition was used for both HR alloys it is worth nothing that the HR-I-1 one becomes nearly eutectic.

RESULTS AND DISCUSSION

Shrinkage size

The resulting shrinkage size values and the main parameters obtained from the cooling curves recorded for each cast iron used to manufacture the test parts are shown in Table 2. A general view of data included in this table shows the strong influence of composition and of inoculation on the shrinkage size. Eutectic temperatures show the usual evolution when adding some inoculant to melts[9,18]

Fig. 2 shows the evolution of the shrinkage areas found in the produced test parts as a function of carbon content and CE. In both graphs, it is observed that the hypereutectic test parts show smaller defects than the corresponding hypoeutectic ones. On the other hand, inoculation of alloys also reduces the size of contraction porosities found in the test parts. These observations agree with previously published results[2,3,4] and with the common results found in ductile iron castings produced in foundry plants.

Taking into account the effects observed in Fig. 2 for the two variables considered above, the two HO-NI test parts showed the biggest shrinkage sizes while the smallest ones were found in the HR-I parts. These results must be related to the different graphite expansion levels expected from the hypoeutectic and non inoculated parts up to the hypereutectic and inoculated ones. Besides when comparing data plotted in Fig. 2 it is observed that carbon content seems to show a higher effect on the shrinkage size than inoculation. According to this, the two HO-I test parts exhibit similar or higher shrinkage areas in Fig. 2 than the HR-NI ones. The big differences observed in the shrinkage areas that correspond to the non-inoculated parts when comparing to the inoculated cases lead to think that other processing variables apart from carbon content and/or CE become important when inoculant is not added to melts. Fig. 2 also shows the values of TELOW for the non inoculated alloys. This parameter has been reported as one of the main indicators to evaluate the graphite nucleation potential of cast irons9. The correlation between TELOW, recalescence (R) and the size of the shrinkage found in the test parts is shown in Fig. 3. Although distribution of data is scattered, the expected positive tendency for reducing the size of the defect is found when increasing TELOW and when decreasing R.

Going back to data plotted in Fig. 2, the HR-NI-1 case shows a large shrinkage area that can be related to a low value of TE_{LOW} and vice versa. However, a different trend is found in the HO-NI alloys despite the defect areas are comparatively quite big in this second case. This fact is probably due to the relevant influence of other variables which have not been considered here.

Interestingly the HR-NI-1 and HR-I-1 alloys represent two cases with intermediate carbon contents (see Table 1) that allow checking the beneficial inoculation effect on shrinkage size reduction. A similar effect can be also detected when comparing HO-NI and HO-I alloys. Inoculant addition shows the smallest influence on defect size for the highest carbon content. These observations can

be explained as being due to the comparatively large graphite expansion exhibited in the high carbon alloys which reduces the positive effect of inoculation when minimizing the shrinkage appearance.

Metallographic characterization of the last solidification zones

Table 3 shows that the inoculant addition certainly increases nodule count for a given composition. Additionally, the central areas of hypereutectic test parts show higher nodule count values than the hypoeutectic ones, both produced with similar inoculation. Thus both high CE and inoculant addition promote alloys with high graphite nodules nucleation along solidification as it was previously reported[5,19,20,21]. These results explain the lowest shrinkage incidence on the hypereutectic and inoculated samples (Fig. 2) as these two alloys would have the biggest graphite expansion to compensate for the metallic contraction during solidification.

When correlating the nodule count data included in Table 3 to the shrinkage size and to TE_{LOW}, the distributions shown in Fig. 4 are obtained. The evolution of the shrinkage size (open circles) agrees with the previous assumption about the positive effect of high graphite nucleation when reducing the incidence of this defect. Only the alloy HR-NI-2 (indicated with an arrow in Fig. 4) shows an anomalous behavior as it has been already noted in Fig. 2.

On the other hand, the evolution of TE_{Low} shows a trend that agrees with the results reported by Larrañaga et al.[9]. However, these authors did not include more detailed information about this tendency. The dotted line in Fig. 4 shows a sharp increase of TE_{Low} for low values of nodule count and a progressive increase for intermediate and high values of this last parameter.

All the inoculated samples show nodularity values higher than 95% while the non-inoculated ones show some graphite particles with irregular shapes (see Fig. 5a and Fig. 5c respectively). Table 3 also shows that all metallic matrices that correspond to the non-inoculated samples contain carbides which the highest content was found in the HO-NI-2 sample by far (Fig. 5d). This sample also contain the highest magnesium content (0.046 wt. %) which has been reported as a promoter of carbides[18]. Fig. 5b shows the matrix composition of the HR-I-2 sample which is free of carbides like the rest of the inoculated alloys prepared in the present work.

Macroscopic and microscopic features of contraction defects

According to the classification of shrinkage defects proposed by Stefanescu[14] (Fig. 6) the different defects found in all test parts produced in this study have been identified as shown in Table 4.
Comparison of results included in Table 4 shows that all four types of defects are present only in the two hypoeutectic and non inoculated cast irons. This fact agrees with the previously observation about the maximum size of shrinkage defects found for these two alloys and the high contraction effect expected in these cases. Inoculation of both hypoeutectic and hypereutectic test parts helps to avoid the formation of microshrinkage while pipe defects and caved surfaces were not detected only when additionally, increasing CE content. Finally, macroporosities appear in all test parts though the size of this type of defect also decreases when increasing CE and/or when adding inoculant.

According to results included in Table 4, inoculation of cast irons has shown to be the most effective process to minimize the appearance of microshrinkage defects.

Regarding the microscopic characteristics of contraction defects, the hypereutectic inoculated test parts only showed shrinkage cavities that were identified as macroporosities with smooth but irregular internal surfaces (Fig. 7). In this figure, it is also seen that a graphite layer is present on the internal surfaces of these cavities. The comparative high CE content exhibited by the hypereutectic cast irons promotes that the remaining liquid during solidification contains very high carbon content. This fact is probably related to the formation of the graphite layer on the internal surfaces of the porosities observed in these test parts.

As it has already stated in Table 4, features of defects found in the HR-NI test parts are different from the HR inoculated ones. In the former case, caved surfaces and an area that contains microshrinkage (this last marked in Fig. 8a with a circle) were detected in addition to macroshrinkage. The inner surfaces of macroporosities showed “rounded dendrites”, with primary and initial secondary arms, covered by a graphite layer (Fig. 8b). When comparing the characteristics of macroporosities found in HR-I and in HR-NI castings it is detected that dendrites are only present in the non inoculated cases as whole contraction effect is expected to be higher in them than for the corresponding inoculated alloys. Fig. 8c shows a detailed view of the internal cavity of a microshrinkage defect which was found in the HR-NI-1 test part. This cavity contains dendrites that are also covered with a graphite layer. Note here that the amount of dendrites development observed in microshrinkage is higher than in case of macroporosities and their shape is more elongated with more sharp endings in the last case, with primary, secondary and initial of tertiary arms. This observation should be related to the formation of microshrinkage during the last steps of solidification.

Once again graphite layer appears stuck to the internal surfaces of both macroshrinkage and microshrinkage defects detected in the hypereutectic test parts despite any inoculant was not added in these two cases. However, it is worthy to stress here that microshrinkage defects were not found in the HR-NI-2 test part. This result is probably related to the higher carbon content exhibited by this alloy (see Table 1) and likely to its higher graphite nucleation level (see Table 2) when comparing to the HR-NI-1 one.

Regarding the hypoeutectic and inoculated alloys, big cavities that are open to air have been found after cutting the two test parts manufactured. These cavities were not detected in any of the hypereutectic castings, they show smooth internal surfaces and they have been considered as pipe defects (open macroshrinkage) according to the classification adopted in Fig. 4.

Additionally, to these pipe defects, the two HO-I parts contain caved surfaces and an important number of close macroporosities as it can be seen in Fig. 9a for the HO-I-1 test part. Surprisingly FESEM inspection of these macroporosities shows two different types of voids. Some of them are quite similar to those found in the hypereutectic non-inoculated test parts, i.e. rounded dendrites and a graphite layer are present in their internal surface (Fig. 9b). However other voids contain rounded dendrites and graphite nodules aggregated to them that seem to be the result of a nearly coupled growth during solidification (Fig. 9c and Fig. 9d). These dendrite-nodules aggregates were already reported by Ruxanda et al.[22] in a microshrinkage defect that was found in fracture surfaces of a

ductile iron plate. Another interesting fact in this second case is the absence of any graphite layer stuck to the inner surfaces.

The characteristics of macroporosities shown in Fig. 9c and Fig. 9d seem to be a consequence of the CE values exhibited by HO-I alloys (see Table 1). According to this hypoeutectic composition solidification should start by forming primary austenite dendrites in the liquidus arrest commonly found in cooling curves. The neighboring liquid areas would increase their carbon content as this element is rejected when austenite phase is formed. Thus, local liquid zones with some level of hypereutectic composition are present close to dendrites and graphite particles precipitation and growth are obtained when cooling. This solidification pattern for ductile irons was already proposed in 1985 by Rickert and Engler[23] and then confirmed by other authors[1,24,25,26]. The lack of any graphite layer in the inner surface of this kind of voids is probably related to the comparatively lower amount of carbon available with respect to HR alloys and to the formation of graphite nodules.

Fig. 9e and Fig. 9f show the results obtained from the EDS microanalyses performed on the inner surface of the void and on the matrix which surrounds it respectively. Carbon peaks were not detected in these spectra and the only difference found when comparing them is the presence of a magnesium peak in the one obtained from the inner surface of the macroporosity (spectrum #1). According to the effects of CE and inoculation observed in the present study, the hypoeutectic and non-inoculated test parts are the most favourable case for obtaining contraction defects. Table 4 certainly confirms this fact and HO-NI test parts contain all four types of contraction defects classified in Fig. 6. Fig. 10a shows a general view of these defects in case of the HO-NI-1 test part.

The examination by FESEM of the microshrinkage present in the HO-NI-1 part shows an inner surface plenty of dendrites (Fig. 10b), like the macroporosity, and with interrupted graphite deposits that cover some areas of these dendrites (Fig. 10c and Fig. 10d). Also, the detailed views in Fig. 10 show shrunk surfaces in the areas located in between the rounded ends of dendrite arms. These shapes can be a consequence of the intense contraction due to the melt hypoeutectic composition in addition to the lack of any inoculation effect. Note that these shrunk surfaces were not detected in the HR-NI parts (see Fig. 8). Regarding the interrupted graphite layers shown in Fig. 10c and Fig. 10d, it is possible that only the very last solidifying liquid has high enough carbon content to promote their precipitation. In the HR-NI case, the comparatively high carbon content available would allow making continuous this graphite layer (see Fig. 8c).

CONCLUSIONS

A group of eight different ductile cast iron alloys have been prepared to analyze the effect of different carbon equivalent contents, inoculation levels and thermal characteristics of solidifying melts on shrinkage size and features. The main conclusions of this work are the following:

1. It has been found that hypereutectic test parts show smaller defects than the corresponding hypoeutectic ones. Additionally, inoculation also reduces the size of shrinkage porosities. Thus, HO-NI test parts have showed the biggest shrinkage size found in the present work while the smallest one has been reported for the HR-I parts. These results are related to the different graphite expansion levels during solidification.

2. Carbon equivalent content has shown a more potent effect on shrinkage size minimization than inoculation. Inoculant addition exhibited a very small influence on defect size in those alloys with the highest carbon content. In addition to this fact, the two HO-I test parts showed higher shrinkage areas than the HR-NI ones. These observations have been considered due to the comparatively large graphite expansion provoked by the high carbon of alloys which hides the positive effect of inoculation.

3. Although both inoculation and high carbon equivalent have a relevant effect on increasing TE_{low} which has been satisfactorily correlated with experimental nodule count, the former parameter has shown to be the most effective. Thus, the HO-I test parts showed higher nodule count values but also bigger shrinkage areas than the HR-NI ones. This observation must be explained due to the comparatively high primary graphite expansion in the HR-NI case that leads to a reduction of "pipe" contraction defects in test parts manufactured with this alloy. On the contrary, both HO-I test parts do not show microshrinkage as secondary graphite nucleation seems to be favored by inoculation when comparing to the HR-NI cases.

4. Inoculation of both hypoeutectic and hypereutectic test parts avoided the formation of microshrinkage while pipe defects and caved surfaces were not detected only when additionally, increasing carbon equivalent content. Macroporosities appear in all test parts though their size decreases when increasing carbon equivalent and/or when adding inoculant.

5. Only macroporosities were detected in the HR-I test parts which show smooth but irregular internal surfaces with a continuous graphite layer related to the hypereutectic composition that promotes high carbon contents in the last solidifying liquid.

6. HR-NI parts contained caved surfaces, microshrinkage and macroporosities. Although the inner surfaces of the two last internal defects show dendrites covered by a continuous graphite layer, the ones found in microshrinkage are numerous and sharp-shaped as they formation takes place in the last stages of solidification.

7. HO-I test parts contained big pipe cavities with smooth internal surfaces that were not found in any of the hypereutectic parts, caved surfaces and an important number of macroporosities were detected as well. FESEM inspection of macroporosities shows two different types of voids: some of them are similar to those found in the HR-NI test parts (with dendrites covered by a graphite layer) and other ones that contain rounded dendrites and graphite nodules aggregated to them without any graphite layer. This last morphology is related to the comparatively low amount of carbon content with respect to the hypereutectic alloys and to the formation of graphite nodules.

8. Hypoeutectic non inoculated parts contained all four types of defects. The internal surfaces of microshrinkage are plenty of dendrites with interrupted graphite deposits and shrunk surfaces in the areas located in between the rounded ends of dendrite arms. This feature has been suggested to be a consequence of an intense contraction due to the hypoeutectic composition in addition to the lack of any inoculation effect.

ACKNOWLEDGMENTS

This work has been financially supported by Fundería Condals S.A foundry and by Catalan Government by awarding the scholarship from AGAUR for the Industrial PhD. The authors thank Centres científics i tecnològics (CCiT) from the Universitat de Barcelona for the collaboration in all the analysis. The authors would like to acknowledge to Dr. Jon Sertucha from IK4-Azterlan for his help during the execution of the present work.

REFERENCES

1. D.M. Stefanescu, *Science and engineering of casting solidification*. Springer, 2015.

2. T. Skaland, *AFS Trans.*(2001): 1073-1084.

3. P. Larrañaga, J. Sertucha, and R. Suárez. REV METAL MADRID 42.4 (2006): 244-255.

4. A. Tadesse, H. Fredriksson, MATER SCI FORUM, Vols. 790-791, pp. 447-451, 2014

5. D. White, (12-081). *AFS Trans.*, 2012, vol. 120, p. 389.

6. T. Skaland, *FTJ* 2004, vol. 178, no 3620, p. 396-400.

7. T. Kanno, et al. *AFS Trans., Vol. 114*, 2006, vol. 114, p. 525-534.

8. R. Suárez, J. M. Gutiérrez, G. Alonso, J. Sertucha, W*FC*, 2012.

9. P. Larrañaga, J. M. Gutiérrez, A. Loizaga, J. Sertucha, R. Suárez, *AFS Trans.*, 2008, vol. 116, pp 547-561.

10. G. Alonso, A. Loizaga, G. Zarrabeitia, D. M. Stefanescu, R. Suarez, *AFS Trans.*, 2014, vol. 122, paper 14-006.

11. D. M. Stefanescu, H. Q. Qiu, C. H. Chen, *AFS Trans.*, 1995, vol. 103, pp 189-197.

12. S. I. Karsay, Ductile Iron: Production Practices, 3rd. ed., AFS Trans., 1985, pp 129.

13. J. F. Wallace, P. K. Samal, J. D. Voss, *AFS Trans.*, vol. 92, 1984, pp 765-784.

14. D. M. Stefanescu, INT J CAST METAL RES, 2005, vol. 18, nº3, pp 129-143.

15. A. S. Sabau, *AFS Trans.*, 2005, vol. 113, paper 05-160.

16. I. Ohnaka, A. Sato, A. Sugiyama, F. Kinoshita, INT J CAST METAL RES, 2008, vol. 21, pp 11-16.

17. ASM Specialty Handbook Cast Irons. *ASM International*, 1996. ISBN. 978-0-87170-564-8.

18. Roy Elliot BSc, PhD. Cast Iron Technology. 1988. ISBN. 0-408-01512-8.

19. J. Campbell, “Complete Casting Handbook”, Elsevier, 2011. DOI: 10.1016/B978-1-85617-809-9.10001-5

20. E. Fraś, H. López, Int J Metalcast. summer 2010.

21. R. Suárez, J. M. Gutiérrez, A. Loizaga, P. Larrañaga y J. Sertucha, REV METAL MADRID, Septiembre-Octubre 2009, 45 (5), pp 339-350.

22. R. Ruxanda, L. Beltran-Sanchez, J. Massone, D. M. Stefanescu, *AFS Trans.*, 2001, vol. 109, paper 01-066.

23. A. Rickert, S. Engler, The Physical Metallurgy of Cast Iron, H. Fredriksson and M. Hillert, Ed., Proc. Materials Research Society, North Holland, vol. 34, 1985, pp 165.

24. D. M. Stefanescu, Cast Iron (in Solidification of Eutectic Alloys), Casting, vol. 15, ASM Handbook, D.M. Stefanescu, Ed., *ASM International*, 1988, pp 168–181.

25. D. K. Bandyopadhyay, D. M. Stefanescu, Physical Metallurgy of Cast Iron IV, G. Ohira, T. Kusakawa, and E. Niyama, Ed., Materials Research Society, 1989, pp 15–26.

26. D. M. Stefanescu, MAT SCI ENG A-STRUCT 413 (2005): pp 322-333.

Table 1. Inoculant additions (wt. %), chemical composition of cast irons (wt. %) and pouring temperatures (ºC) used in the present work.

Alloy	Inoculant	CE*	C	Si	Mn	S	P	Cr	Cu	Mg	T
HR-I-1	0.30	4.33	3.61	2.26	0.38	0.004	0.022	0.044	0.24	0.032	1380
HR-I-2	0.30	4.60	3.73	2.73	0.36	0.004	0.022	0.051	0.37	0.036	1385
HR-NI-1	0	4.42	3.61	2.55	0.34	0.004	0.021	0.042	0.23	0.033	1356
HR-NI-2	0	4.45	3.78	2.11	0.30	0.005	0.025	0.044	0.13	0.036	1377
HO-I-1	0.30	4.18	3.44	2.32	0.40	0.007	0.022	0.063	0.26	0.027	1410
HO-I-2	0.10	4.08	3.44	2.01	0.36	0.004	0.023	0.056	0.20	0.030	1397
HO-NI-1	0	4.18	3.44	2.32	0.40	0.007	0.022	0.063	0.26	0.027	1410
HO-NI-2	0	4.22	3.49	2.31	0.29	0.008	0.019	0.039	0.10	0.046	1399

*CE = %C + 0.31%Si - 0.027%Mn + 0.076%Cu + 0.33%P + 0.4%S (eutectic composition at 4.30%)[17]

Table 2. Measured shrinkage areas and parameters obtained from cooling curves.

Alloy	Inoculated samples			Non inoculated samples			Shrinkage
	T_L (ºC)	TE_{LOW} (ºC)	R (ºC)	T_L (ºC)	TE_{LOW} (ºC)	R (ºC)	(mm^2)
HR-I-1	1156.6	1147.4	1.4	-	-	-	12
HR-I-2	1151.6	1151.1	2.2	-	-	-	16
HR-NI-1	-	-	-	1149.4	1124.9	12.2	207
HR-NI-2	-	-	-	1138.8	1138.1	2.8	30
HO-I-1	1185.4	1147.2	2.5	-	-	-	207
HO-I-2	1189.7	1146.1	2.4	-	-	-	170
HO-NI-1	-	-	-	1180.2	1118.3	4.2	281
HO-NI-2	-	-	-	1171.3	1138.5	5.9	349

Table 3. Metallographic characterization of central zones of test parts.

Alloy	Inoculation (wt. %)	Nodule count (mm^{-2})			f_c	f_α	f_p
		Average	min	max			
HR-I-1	0.30	505	480	530	0	45	55
HR-I-2	0.30	530	505	550	0	30	70
HR-NI-1	0	45	40	50	15	30	55
HR-NI-2	0	60	55	65	10	30	60
HO-I-1	0.30	395	345	470	0	60	40
HO-I-2	0.10	255	235	270	0	15	85
HO-NI-1	0	45	40	50	10	20	70
HO-NI-2	0	25	20	30	30	20	50

Table 4. Classification of the shrinkage defects found in the test parts manufactured in the present work.

Test part	Pipe	Caved surface	Macroporosity	Microshrinkage
HR-I-1	no	no	**yes**	no
HR-I-2	no	no	**yes**	no
HR-NI-1	no	**yes**	**yes**	**yes**
HR-NI-2	no	**yes**	**yes**	no
HO-I-1	**yes**	**yes**	**yes**	no
HO-I-2	**yes**	**yes**	**yes**	no
HO-NI-1	**yes**	**yes**	**yes**	**yes**
HO-NI-2	**yes**	**yes**	**yes**	**yes**

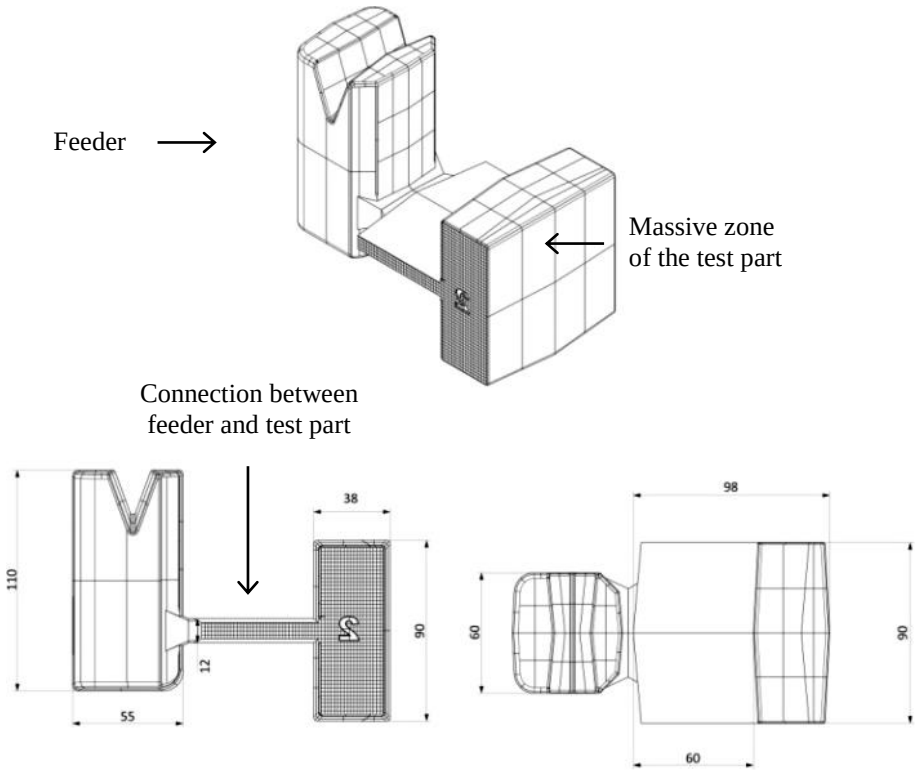

Fig. 1. Test part and riser lay-out used in the experimental work.

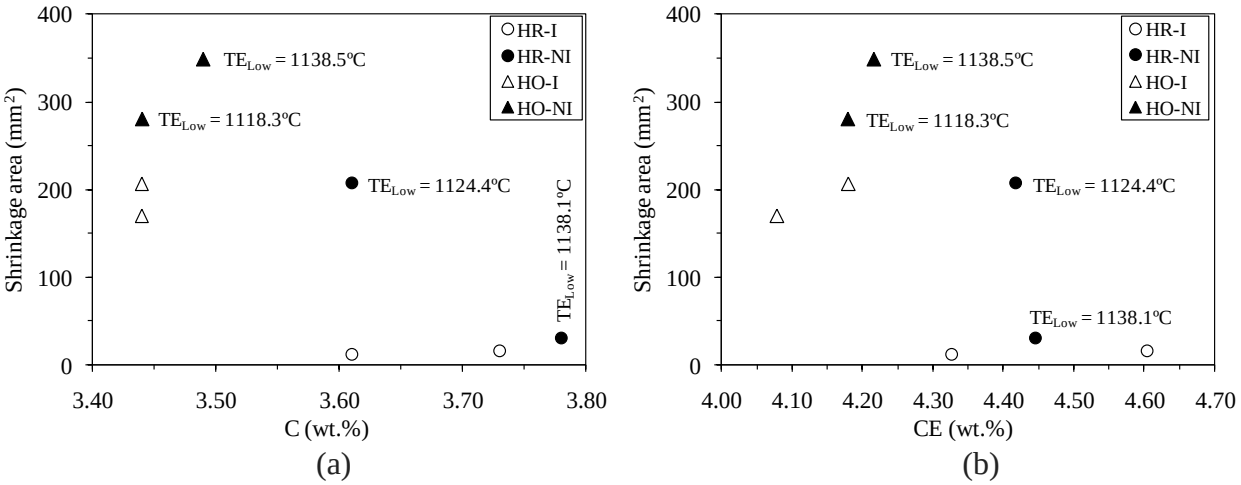

(a) (b)

Fig. 2. Evolution of the shrinkage size with (a) carbon content and (b) CE.

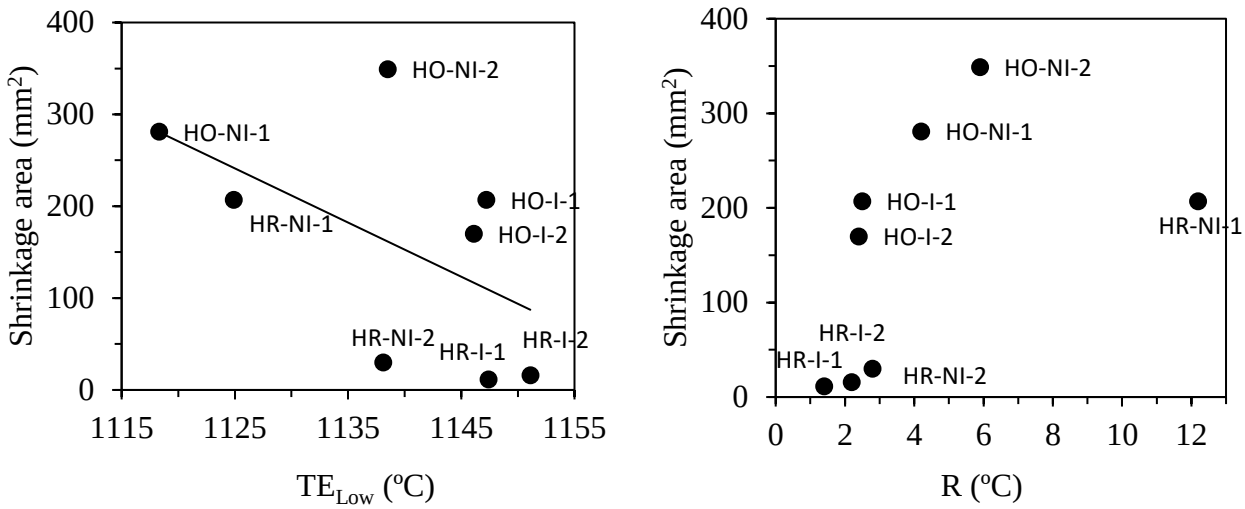

Fig. 3. Evolution of the shrinkage size with TE_{LOW} and R

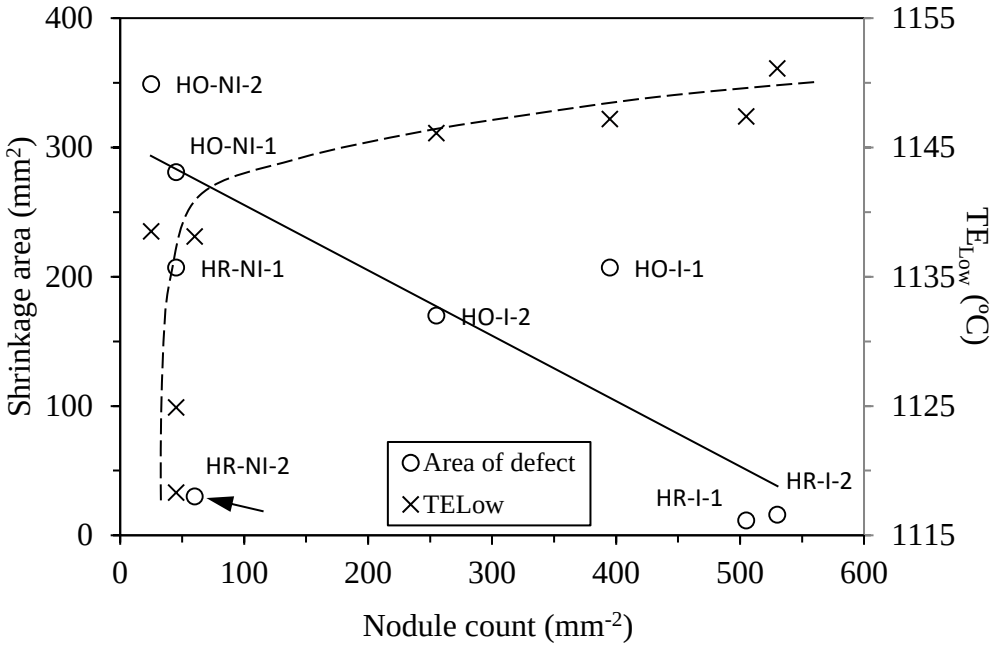

Fig. 4. Evolution of the shrinkage size and TE_{Low} with nodule count.

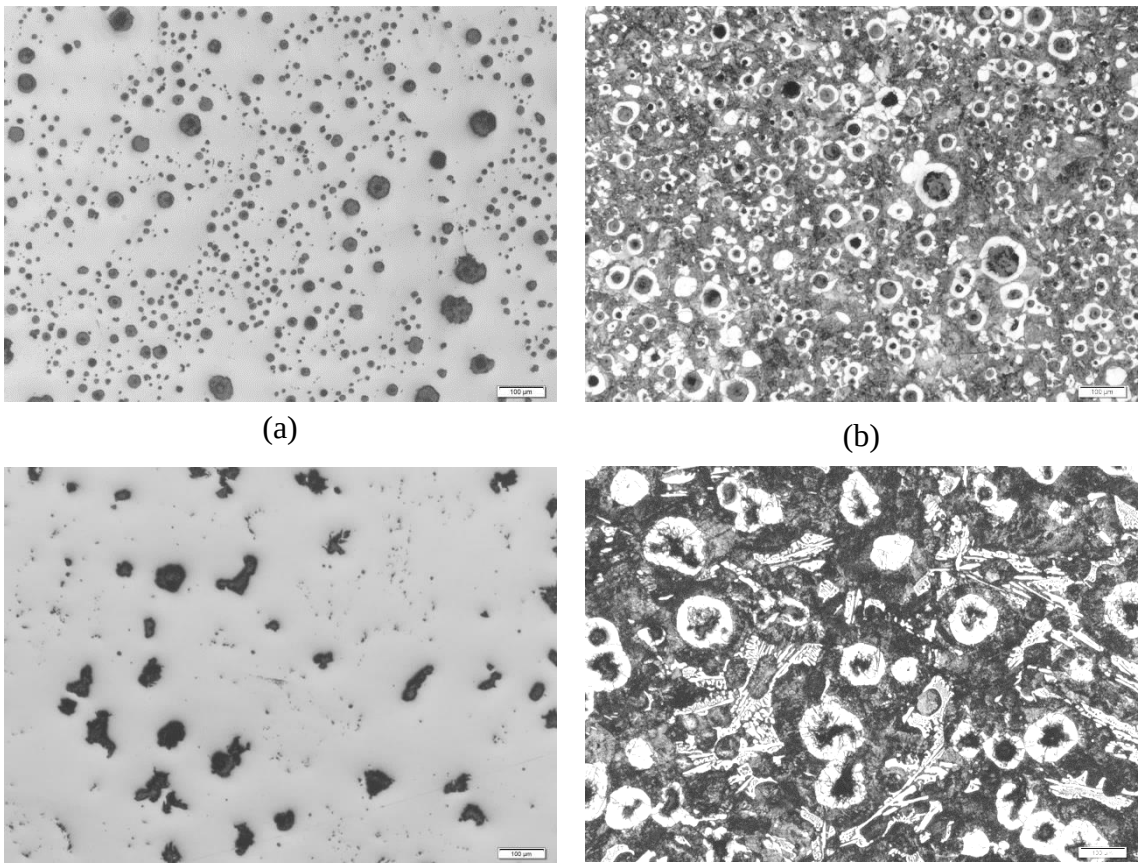

(a) (b)

(c) (d)

Fig. 5. Graphite particles in the a) HR-I-2 sample and c) HO-NI-2 sample. Matrix composition of b) HR-I-2 sample and d) HO-NI-2 sample.

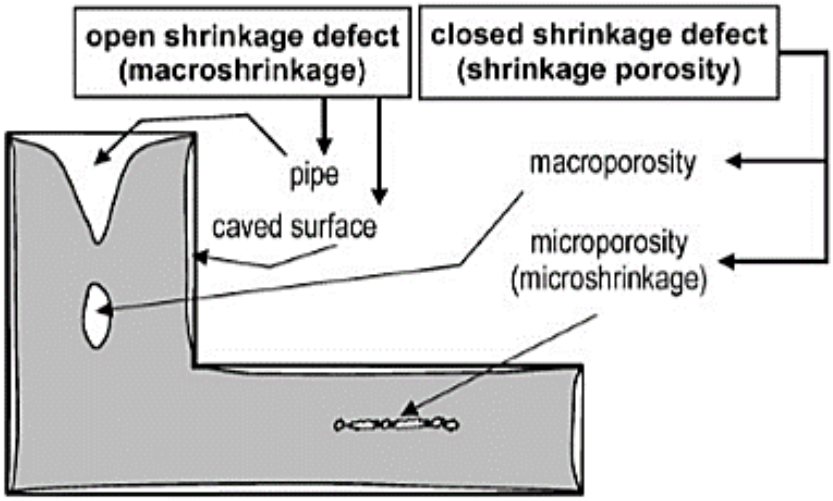

Fig. 6. Classification of the different shrinkage defects found in cast irons[14].

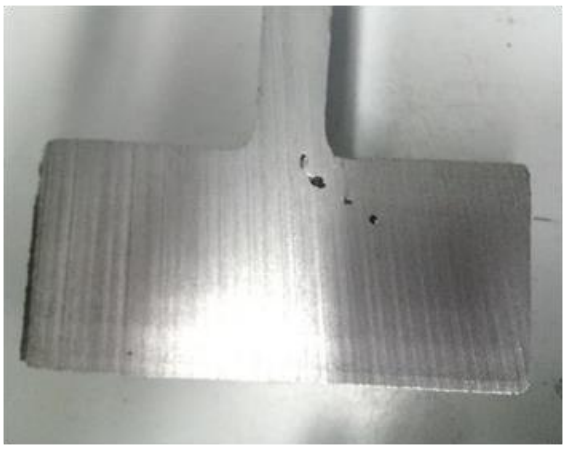

(a)

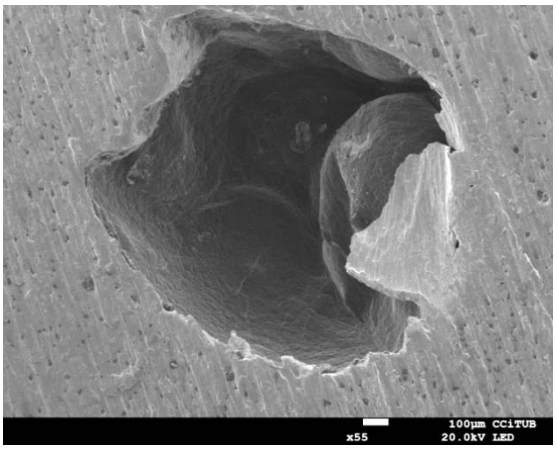

(b)

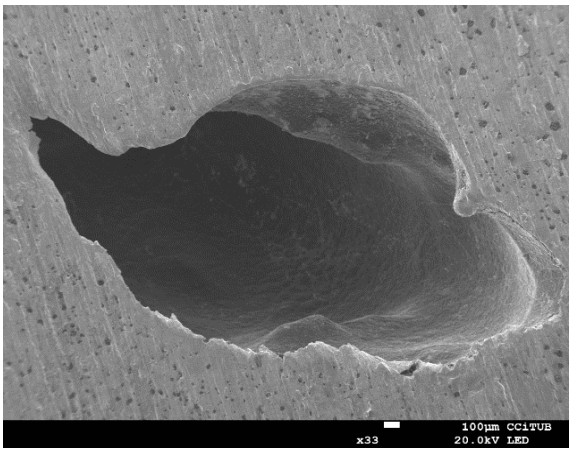

(c)

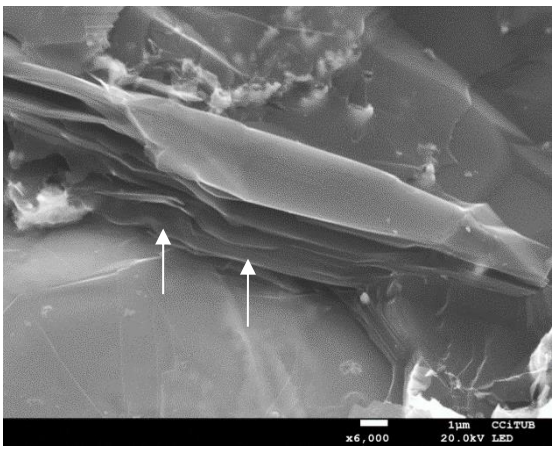

(d)

Fig. 7. Macroporosities found in the HR-I-1 test part: a) general view, b) and c) FESEM micrograph of two cavities and d) detail of the graphite layer found in the internal surface (arrows).

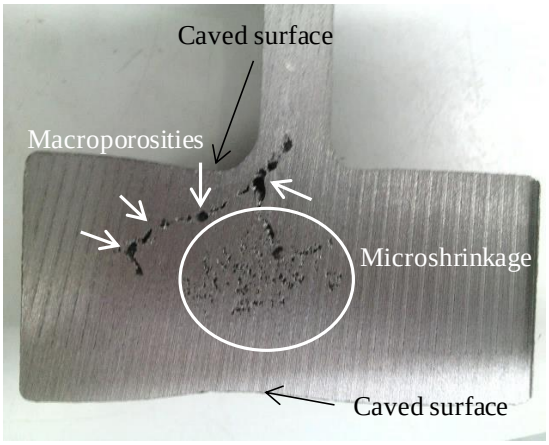

(a)

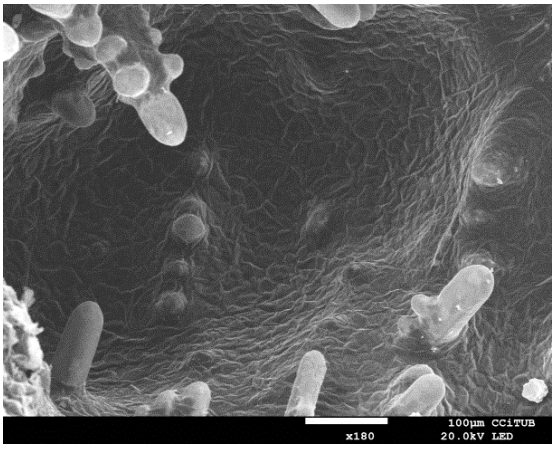

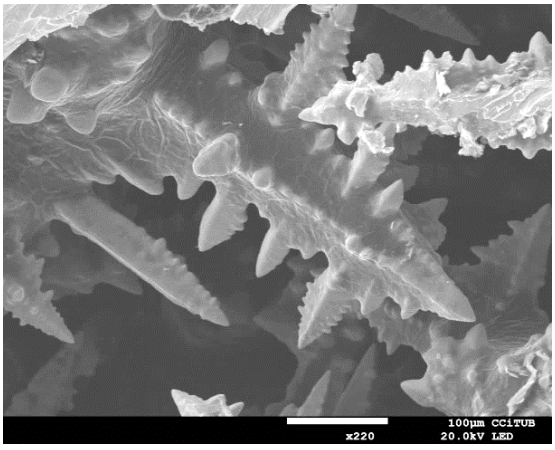

(b) (c)

Fig. 8. Contraction defects found in the HR-NI-1 test part: a) general view, b) FESEM micrograph of the internal cavity of a macroporosity and c) of a microshrinkage defect.

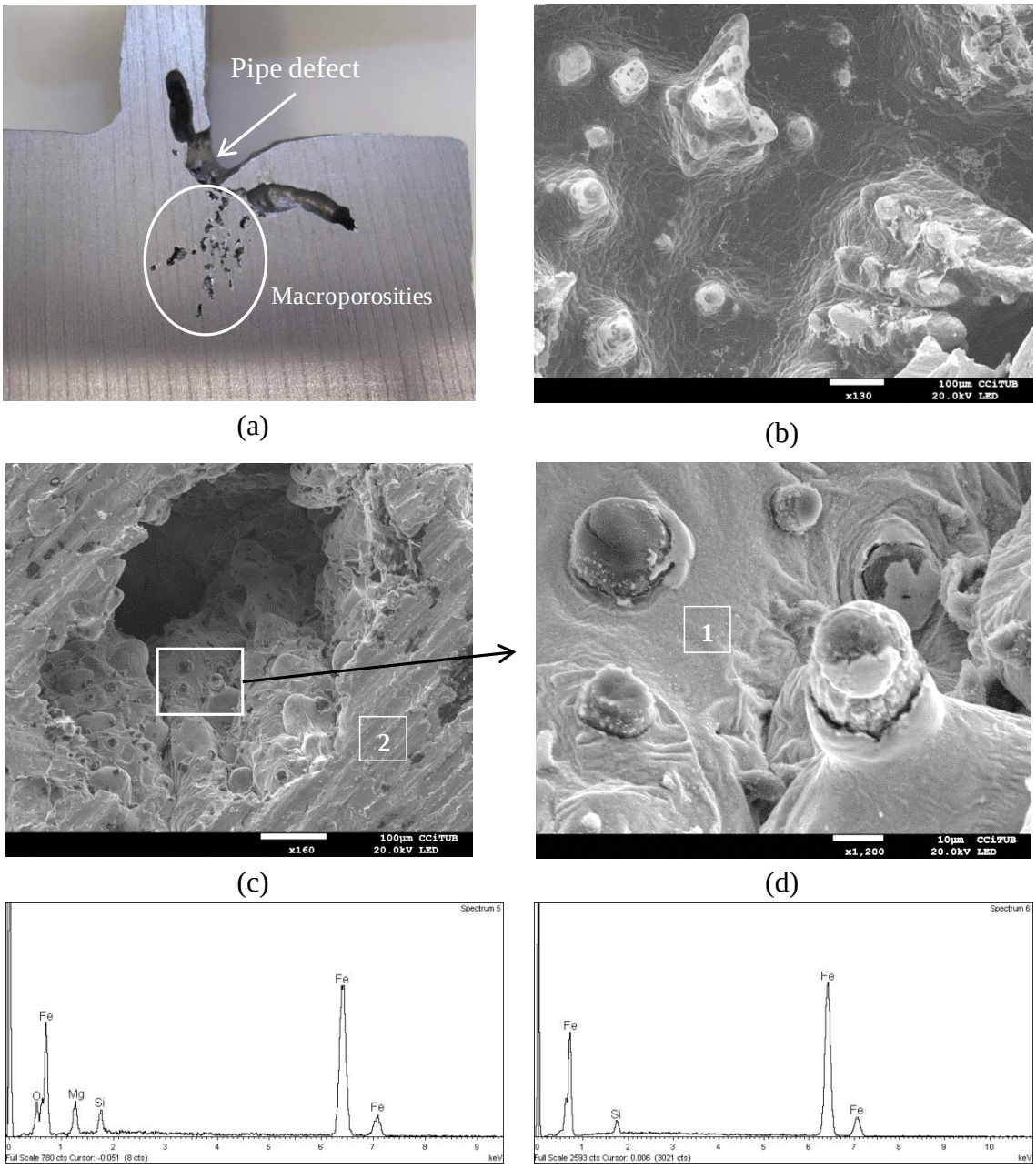

Fig. 9. a) General view of one half cut from the HO-I-1 test part, b) FESEM micrograph of a macroporosity with dendrites and the graphite layer, c) and d) FESEM micrographs of a macroporosity that contains coupled dendrites and graphite nodules, e) EDS microanalysis of the inner surface marked as #1 in micrograph d), and f) EDS microanalysis of the matrix surrounding the macroporosity (area marked as #2 in micrograph c)).

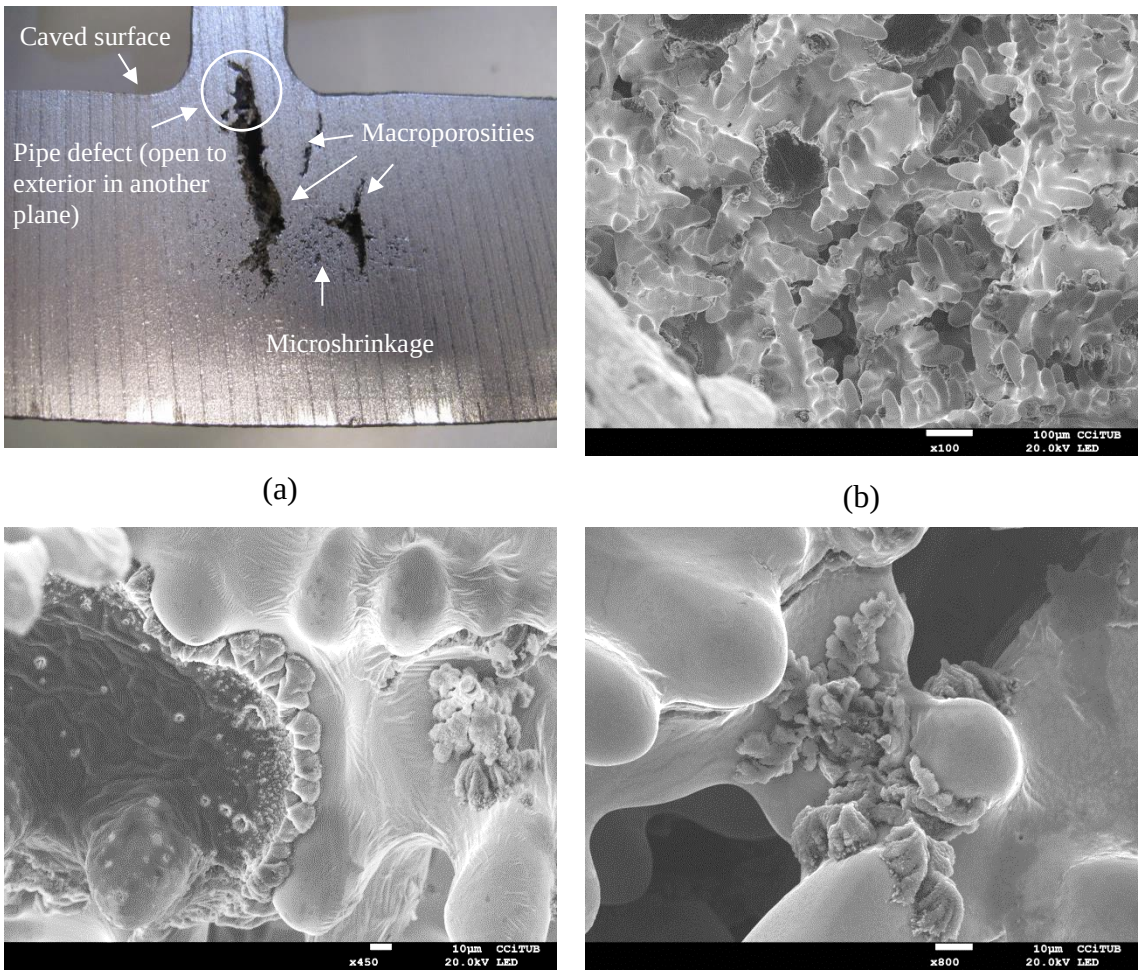

(a) (b)

(c) (d)

Fig. 10. a) General view of defects found in the HO-NI-1 test part, b) FESEM micrograph of the dendrites found in the internal surface of a microshrinkage, c) and d) detailed views of the graphitic aggregates deposited in the dendrites.